



Spatial and temporal joint, partially-joint and individual sources in independent component analysis: Application to social brain fMRI dataset



Mansoor Pakravan*, Mohammad Bagher Shamsollahi

Department of Electrical Engineering, Sharif University of Technology, Tehran, Iran

ARTICLE INFO

Keywords:

Joint analysis
Multi-subject dataset
Joint, partially-joint and individual sources
Independent component analysis

ABSTRACT

Background Three types of sources can be considered in the analysis of multi-subject datasets: (i) joint sources which are common among all subjects, (ii) partially-joint sources which are common only among a subset of subjects, and (iii) individual sources which belong to each subject and represent the specific conditions of that subject. Extracting spatial and temporal joint, partially-joint, and individual sources of multi-subject datasets is of significant importance to analyze common and cross information of multiple subjects.

New method: We present a new framework to extract these three types of spatial and temporal sources in multi-subject functional magnetic resonance imaging (fMRI) datasets. In this framework, temporal and spatial independent component analysis are utilized, and a weighted sum of higher-order cumulants is maximized.

Results: We evaluate the presented algorithm by analyzing simulated data and one real multi-subject fMRI dataset. Our results on the real dataset are consistent with the existing meta-analysis studies. We show that spatial and temporal jointness of extracted joint and partially-joint sources in the theory of mind regions of brain increase with the age of subjects.

Comparison with existing method: In Richardson et al. (2018), predefined regions of interest (ROI) have been used to analyze the real dataset, whereas our unified algorithm simultaneously extracts activated and uncorrelated ROIs, and determines their spatial and temporal jointness without additional computations.

Conclusions: Extracting temporal and spatial joint and partially-joint sources in a unified algorithm improves the accuracy of joint analysis of the multi-subject fMRI dataset.

1. Introduction

Blind source separation techniques extract a set of maximally independent “components” from their linear mixtures. These techniques have been successfully used in analyzing brain imaging data, especially functional magnetic resonance imaging (fMRI) data (Calhoun and Adali, 2006). For example, blind source separation techniques have been exploited to investigate functional connectivity (Beckmann et al., 2005), identify temporally coherent networks (Calhoun et al., 2008), analyze visual perception (Calhoun et al., 2001a), cinema viewing task (Pamilo et al., 2012), and remove artifact (Du et al., 2016).

Independent component analysis (ICA) (Comon and Jutten, 2010) is one of these techniques in which the maximal independence can be achieved in space (voxels in fMRI data) and time (blood oxygen level dependent signal), and accordingly two types of ICA applications in fMRI datasets are obtained: spatial ICA and temporal ICA (Calhoun et al., 2001c). For the first time in McKeown et al. (1998), spatial ICA has been used on fMRI data to decompose it into spatially independent

components to distinguish between non-task-related signal components, movements, and other artifacts. This spatial decomposition can be utilized in the localization paradigm of classical neuroscience and has widely received much attention in the fMRI community. This is because typical fMRI data has many more voxels than time points and can better estimate higher-order statistics or non-Gaussianity across the spatial domain. Especially, the benefits of spatial ICA are further pronounced if individual component maps are largely non-overlapping (Calhoun et al., 2001c), and it extracts spatial pattern with high accuracy for typical cognitive activation paradigms because of the sparse distributed nature of sources (McKeown et al., 1998).

In the temporal approach, BOLD signals can be considered in some seeds in the brain. The seed can be a collection of voxels that are functionally correlated based on prior fMRI studies and its time-course can be the average of the time-courses from those voxels. This seed selection method is simple because it pinpoints directly the voxel regions, but it requires prior knowledge of seeds whose representativeness is not always reliable (Sohn et al., 2015). Note that there are other

* Corresponding author.

E-mail addresses: mpakravan@ee.sharif.edu (M. Pakravan), mshams@sharif.edu (M.B. Shamsollahi).

<https://doi.org/10.1016/j.jneumeth.2019.108453>

Received 27 April 2019; Received in revised form 25 September 2019; Accepted 30 September 2019

Available online 20 October 2019

0165-0270/ © 2019 Elsevier B.V. All rights reserved.

methods available for seed selection. One approach is to use data-driven analysis such as spatial ICA (Cole et al., 2010; Wu et al., 2018) to assign each seed to one spatial source. However, the problem of applying separate spatial ICA decompositions for each subject is that the correspondence between estimated spatial components across subjects must be identified. In order to avoid this problem, one solution is to use group analysis to extract spatial sources that are joint across all subjects (Calhoun et al., 2001b; Hotelling, 1936; Adali et al., 2014).

Recently, in Lock et al. (2013), Zhou et al. (2016), and Pakravan and Shamsollahi (2018) multi-subject brain datasets have been analyzed by extracting two types of hidden spatial sources (joint and individual sources). In Lock et al. (2013), the joint and individual variation explained method has been proposed to extract both joint and individual sources. This method is an extension of principal component analysis and extracts common variations between datasets. In Zhou et al. (2016), common orthogonal basis extraction and common nonnegative feature extraction algorithms have been proposed which are matrix factorization problems. It is worth mentioning that common orthogonal basis extraction and common nonnegative features extraction algorithms have a direct connection to group principal component analysis and group ICA and are generally combined with a blind source separation method (Zhou et al., 2016). In Pakravan and Shamsollahi (2018), joint/individual Thin ICA algorithm has been used, which is inspired by the thin ICA algorithm (Cruces and Cichocki, 2003). In Pakravan and Bagher Shamsollahi (2019), higher order cumulants have been used to extract joint, partially-joint, and individual sources of fMRI datasets. To the best of our knowledge, so far no study has analyzed both temporal and spacial joint, partially-joint, and individual sources of multi-subject datasets.

In this study, we use a joint blind source separation algorithm using temporal ICA and spatial ICA approaches. We consider three types of spatial and temporal sources: joint (common across all of the datasets), partially-joint (common in a subset of datasets), and individual (specific for each dataset) sources. This source model is referred to as joint/partially-joint/individual multi-dataset multidimensional (JpJI-MDM). In the spatial ICA approach, after extracting spatial sources (significant clusters of voxels) that are joint or partially joint, we select some seeds in these clusters to analysis blood oxygen level dependent (BOLD) signals of fMRI data with the temporal ICA approach and extract temporal joint sources. We also introduce two new features for each extracted source, referred to as temporal and spatial joint/partially-joint/individual features (JpJI-F), which represent the shape of that source (in terms of higher-order cumulants) and the amount of its jointness.

The algorithm is used to analyze simulated and real fMRI datasets. The results of our analysis on both simulated and real fMRI data demonstrate the benefits of the algorithm as either a complementary or alternative method for the inference of fMRI group data. Furthermore, this algorithm can provide a useful interpretation of multi-subject fMRI data and help to deal with more complex and realistic source models.

The structure of the paper is as follows. Section 2 is devoted to present the method including source model, source extraction method, source type determination, and the spatial and temporal approaches. In Section 3, simulated and real fMRI data are analyzed and the numerical results are reported. Finally, in Sections 4 and 5, the results of our paper are discussed and conclusion remarks are presented, respectively.

2. Method

2.1. Source model

In the JpJI-MDM model, a multi-subject dataset is considered with K subjects, where k th subject has $C_1^{(k)}$, $C_2^{(k)}$, and $C_3^{(k)}$ joint, partially-joint, and individual sources, respectively. Without loss of generality we assume that all subjects have the same number of joint, partially-joint, and individual sources, i.e., $C_1^{(k)} = C_1$, $C_2^{(k)} = C_2$, and $C_3^{(k)} = C_3$. Let C denote the total number of sources for each subject, then we have

$$C = C_1 + C_2 + C_3.$$

We define $\mathcal{K}_{c,k}$ as a subset of subjects which their c th source is joint with the c th source of the k th subject ($\mathbf{y}_c^{(k)}$), and $n_{\mathcal{K}_{c,k}}$ is the number of subjects in $\mathcal{K}_{c,k}$. Therefore, according to the JpJI-MDM model, if $\mathbf{y}_c^{(k)}$ is joint, then $K - 1$ sources exist in other datasets that are similar to $\mathbf{y}_c^{(k)}$ ($n_{\mathcal{K}_{c,k}} = K - 1$). On the other hand, for partially-joint and individual sources we have $n_{\mathcal{K}_{c,k}} < K - 1$ and $n_{\mathcal{K}_{c,k}} = 0$, respectively.

It is worth mentioning that we can use the JpJI-MDM model in clustering schemes by using the extracted partially-joint sources. This is due to the property of the algorithm which can align joint sources across datasets, as a result, there is no permutation indeterminacy across datasets (i.e., joint sources have similar source index in all related datasets).

2.2. Source extraction method

Let $X^{(k)} \in \mathbb{R}^{N \times W}$ represent the observation signal of k th dataset, then the mixing matrix ($A^{(k)} \in \mathbb{R}^{N \times C}$) and source matrix ($S^{(k)} \in \mathbb{R}^{C \times W}$) are related to observation matrix as follows

$$X^{(k)} = A^{(k)} S^{(k)}, \quad k = 1, \dots, K. \quad (1)$$

where W is the length of each source, N is the number of observation's vectors, and C is the number of source's vectors. Here, we assume that the vectors of $S^{(k)}$ are mutually independent with unit variance and zero mean. The mixing matrices $A^{(k)}$; $k = 1, \dots, K$ are also full-column rank.

In the first step, we generate the preprocessed observations matrices ($Z^{(k)}$) as follows (Comon and Jutten, 2010)

1. Dimension reduction with applying the principle component analysis.
2. Employing a pre-whitening system ($W_w^{(k)} = R_{X^{(k)}}^{-1/2}$), where $R_{X^{(k)}}$ is the covariance matrix of $X^{(k)}$.

In the algorithm, two approaches can be used in analyzing multi-subject fMRI datasets, referred to as JpJI spatial ICA (JpJI-sICA) and JpJI temporal ICA (JpJI-tICA). These approaches use a cost function based on higher-order cumulants and deflation framework (Comon and Jutten, 2010).

The following metric is applied to extract the c th source of k th dataset as follows

$$Y_{\mathcal{K}}(\mathbf{y}_c^{(k)}(w)) = \sum_{\eta} \alpha_{\eta} \sum_{k_1, \dots, k_{\eta-1} \in \mathcal{K}} |\text{cum}[\mathbf{y}_c^{(k)}(w), \mathbf{y}_c^{(k_1)}(w), \dots, \mathbf{y}_c^{(k_{\eta-1})}(w)]|^2 \quad (2)$$

where $\eta = 2, 3, 4$. Let $\mathcal{K} = \{1, \dots, K\}/k$. In (2), k_i s for $i = 1, \dots, \eta - 1$ denote $\eta - 1$ subjects that are selected randomly from \mathcal{K} . We also assume $K > \eta - 1$. In addition, the operator $|\cdot|^2$ denotes the squared norm, $\alpha_{\eta} > 0$ is the weight of the η th order cumulant, $\mathbf{y}_c^{(k)}(w) = \mathbf{u}_c^{(k)} Z^{(k)}(w)$ for $w = 1, \dots, W$ represents the estimated source, in which $\mathbf{u}_c^{(k)}$ denotes the c th row of the estimated inverse of mixing matrix, and $Z^{(k)}(w) \in \mathbb{R}^{C \times 1}$ represents the w th vector of preprocessed observation signal.

In this study, only second, third, and fourth-order cumulants are used. In Eq. (2), the cross cumulant of datasets whose c th source is not joint or partially-joint is zero (or very low), because the cross-cumulant of statistically independent random variables is zero. Thus, in Eq. (2), only subjects that are members of $\mathcal{K}_{c,k}$, are important, and we have

$$Y_{\mathcal{K}_{c,k}}(\mathbf{y}_c^{(k)}(w)) = \sum_{\eta} \alpha_{\eta} \sum_{\bar{k}_1, \dots, \bar{k}_{\eta-1} \in \mathcal{K}_{c,k}} |\text{cum}[\mathbf{y}_c^{(k)}(w), \mathbf{y}_c^{(\bar{k}_1)}(w), \dots, \mathbf{y}_c^{(\bar{k}_{\eta-1})}(w)]|^2. \quad (3)$$

Clearly, if $\mathcal{K}_{c,k}$ has no member, it means that the c th source is an individual source in k th dataset, and the cost function is zero. In this case, we set $\mathcal{K} = \{k\}$, and use (2) to extract individual sources. In fact, the cost function for individual sources converts to the thin ICA cost

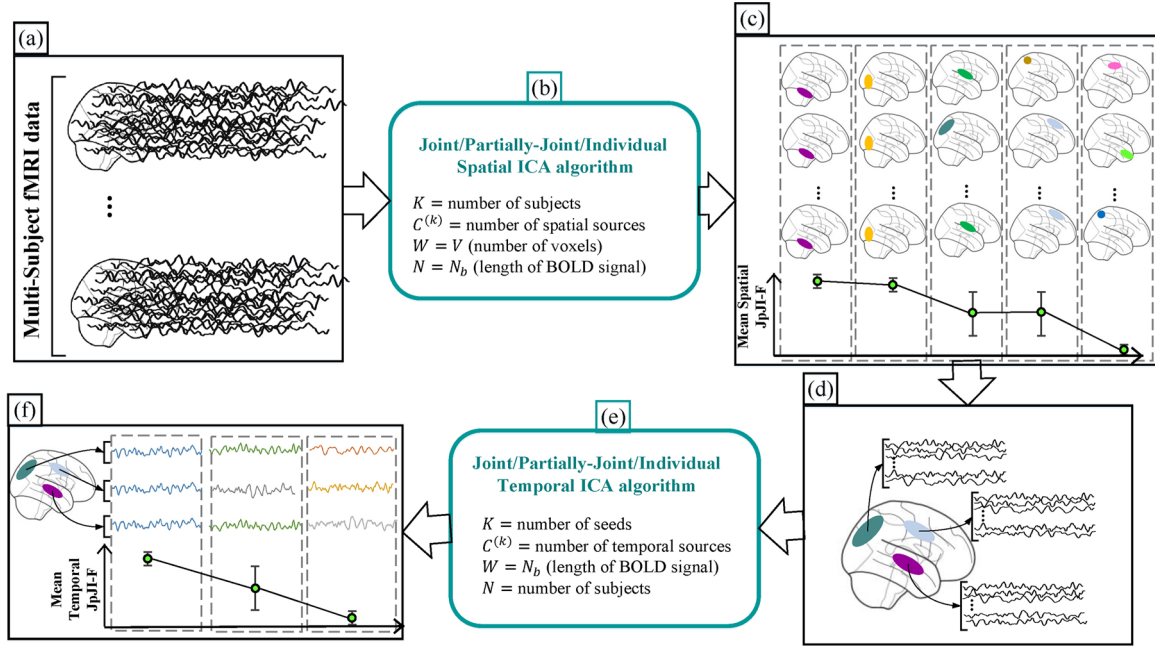


Fig. 1. The joint/partially-joint/individual spatial and temporal independent component analysis (JpJI-sICA and JpJI-tICA). (a) multi-subject fMRI data, (b) dimensions in JpJI-sICA approach, (c) output of JpJI-sICA approach including spatial joint, partially-joint, and individual sources with their spatial JpJI-F, (d) important seeds extracted from JpJI-sICA approach with their time-courses, (e) dimensions in JpJI-tICA approach, (c) output of JpJI-tICA approach including temporal joint, partially-joint, and individual sources with their temporal JpJI-F.

function (Cruces and Cichocki, 2003), which is given by

$$\Upsilon(y_c^{(k)}(w)) = \sum_{\eta} \alpha_{\eta} |\text{cum}[y_c^{(k)}(w), y_c^{(k)}(w), \dots, y_c^{(k)}(w)]|^2. \quad (4)$$

It is worth mentioning that in order to extract desired sources and to align joint sources across subjects, it is not necessary to determine $\mathcal{K}_{c,k}$ for each c th source in k th subject, because the algorithm automatically converts the cost function from Eq. (2) to Eq. (3).

Hereafter, $\Upsilon_{\mathcal{K}}(y_c^{(k)}(w))$ for $\mathcal{K} = \{1, \dots, K\}/k$ is referred to as JpJI-F. It is straightforward to prove that the JpJI-F of the c th source vector ($y_c^{(k)}$) has a linear relation with $n_{\mathcal{K}_{c,k}}$ and if $y_c^{(k)}$ is joint, then its JpJI-F is bigger than when it is partially-joint.

Thanks to the cost function in Eq. (2), the permutation indeterminacy across datasets is resolved, and dependent sources are automatically grouped across datasets. Furthermore, in this method, parameters C_1 , C_2 and C_3 are not necessary to be known for each dataset, because the algorithm automatically determines the type of each source.

It is simple to show that one can use the local maximum of Eq. (2) to extract one of the independent sources (similar to Theorem 1 in Pakravan and Shamsollahi (2018)). This algorithm maximizes the cost function with respect to the first source in the $\text{cum}[\cdot]$ function (i.e., its first input argument) by assuming that other sources are fixed (even in cases that the first source is repeated in the other input arguments of the $\text{cum}[\cdot]$ function). In addition, the optimization is performed with respect to $\mathbf{u}_c^{(k)}$ and accordingly the desired source, $y_c^{(k)*}(w)$, is estimated (i.e., $y_c^{(k)*}(w) = \mathbf{u}_c^{(k)*} Z^{(k)}(w)$). Thus, the optimization problem is $\mathbf{u}_c^{(k)*} = \text{argmax}_{\mathbf{u}_c^{(k)}} \Upsilon_{\mathcal{K}}(y_c^{(k)}(w))$. For simplicity, we rewrite the cost function as follows

$$\Upsilon_{\mathcal{K}}(y_c^{(k)}(w)) = \mathbf{u}_c^{(k)H} M_w^{(\mathcal{K})} \mathbf{u}_c^{(k)}, \quad (5)$$

in which

$$M_w^{(\mathcal{K})} = \sum_{\eta} \alpha_{\eta} \sum_{k_1, \dots, k_{\eta-1} \in \mathcal{K}} C_w^{(\mathcal{K})}(\eta) (C_w^{(\mathcal{K})}(\eta))^H, \quad (6)$$

where

$$C_w^{(\mathcal{K})}(\eta) = \text{cum}[Z^{(k)}(w), y_c^{(k_1)}(w), \dots, y_c^{(k_{\eta-1})}(w)]. \quad (7)$$

In (6) and (7), we observe that $M_w^{(\mathcal{K})}$ is independent of $\mathbf{u}_c^{(k)}$, thus, the maximum of $\Upsilon_{\mathcal{K}}(y_c^{(k)}(w))$ can be obtained by determining the corresponding eigenvector of the dominant eigenvalue of $M_w^{(\mathcal{K})} \in \mathbb{R}^{C \times C}$, where the optimum value of $\mathbf{u}_c^{(k)}$ is the corresponding eigenvector which can be determined by using one or more iterations of any standard methods of finding eigenvalues, e.g., subspace iteration method (SIM) (Saad, 2011).

It should be noted that for individual sources ($\mathcal{K} = \{k\}$), $M_w^{(\mathcal{K})}$ is given by $\sum_{\eta} \alpha_{\eta} C_w^{(k)}(\eta) (C_w^{(k)}(\eta))^H$ where $C_w^{(k)}(\eta) = \text{cum}[Z^{(k)}(w), y_c^{(k)}(w), \dots, y_c^{(k)}(w)]$.

2.3. Source type determination

We use JpJI-F to determine the type of extracted latent sources. As mentioned, the JpJI-F is a metric for the shape of each source and the amount of its jointness with other sources in other subjects. Since the JpJI-F of joint or partially-joint sources is high, if this metric is greater than the threshold σ_0 , it means that the corresponding source is joint or partially-joint. On the other hand, the JpJI-F of individual sources is less than the threshold σ_0 . The parameter σ_0 is a given threshold.

Furthermore, we use the shape of sources to discriminate joint and partially-joint sources. If the minimum of the cross-correlation of extracted sources in all datasets is higher than $\sigma_{\text{similarity}} = 0.98$ that sources are joint, otherwise they are partially-joint sources. In analyzing real dataset, we apply *one-sided t-test* or *two-sided t-test* to find significant clusters in the predefined groups of datasets. If significant clusters can be found, it means that the sources are partially-joint.

2.4. Spatial and temporal approaches

Let V and N_b denote the number of voxels in an fMRI image and the number of time samples in an observed BOLD signal, respectively. The number of independent components (C), for spatial ICA and temporal ICA approaches are N_{sica} and N_{tica} , respectively, and K is the number of subjects.

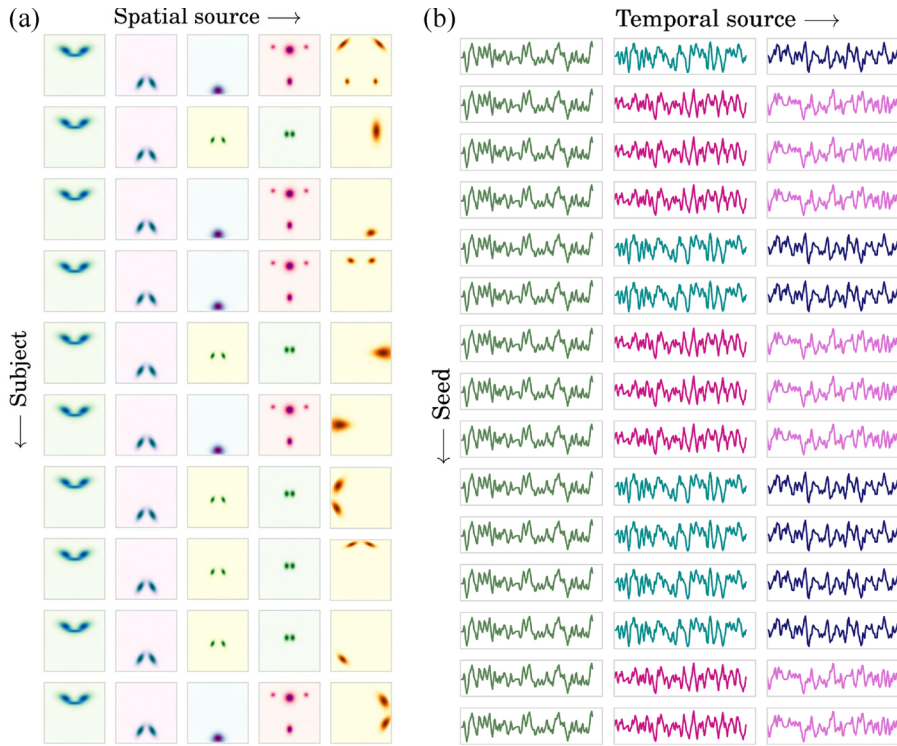


Fig. 2. An example for 2-class JpJI-MDM source model for simulated fMRI data (a) in spatial approach with $C_1 = 2$, $C_2 = 2$, $C_3 = 1$, $W = 64 \times 64$, and $K = \text{number of subjects} = 10$, (b) in temporal approach with $C_1 = 1$, $C_2 = 2$, $C_3 = 0$, $W = 150$, and $K = \text{number of seeds} = 16$. In partially-joint sources in both spatial and temporal approach, there are two clusters of datasets that have similar joint sources.

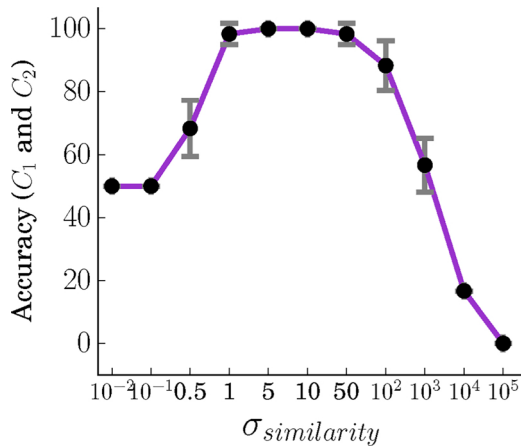


Fig. 3. Performance of JpJI-sICA algorithm versus $\sigma_{similarity}$ ($K = 16$, $C_1 = C_2 = C_3 = 1$) in terms of its accuracy to estimate the number of joint and partially-joint sources.

In JpJI-sICA, datasets are subjects ($K = N_{sub}$) and the vectorized versions of fMRI source images (or volumes) are processed ($W = V$). Observations and source matrices have $[N_b \times V]$ and $[N_{sica} \times V]$ dimensions, respectively. Hereafter, the JpJI-F of this approach is referred to as spatial JpJI-F.

In JpJI-tICA, to reduce complexity, BOLD signals are processed ($W = N_b$) in predefined seeds in some brain regions of interest (ROIs). In this study, we use the results of JpJI-sICA algorithm to find important ROIs (joint or partially-joint) and determine the time-course of each ROI's seed as the average of the time-course of all voxels within that ROI. In this approach, datasets are seeds ($K = N_{seed}$). The observations are made by concatenating each seed's time-course of all subjects in a matrix. Therefore, observation and source matrix have $[N_{sub} \times N_b]$ and $[N_{tica} \times N_b]$ dimensions, respectively. We assume that the number of subjects is greater than N_{tica} . We refer to JpJI-F of this approach as temporal JpJI-F.

Fig. 1 schematically illustrates the algorithm, where in Fig. 1(a) multi-subject fMRI data are shown. In JpJI-sICA approach, we set K to be the number of subjects (Fig. 1(b)), and it extracts joint spatial sources and computes spatial JpJI-F (Fig. 1(c)). The outputs of this approach are ROIs that are joint across all or a subset of subjects.

On the other hand, in JpJI-tICA approach (Fig. 1(e)) we set K to be the number of seeds that are extracted by JpJI-sICA (Fig. 1(d)), and it extracts joint temporal sources in all or a subset of seeds and computes temporal JpJI-F (Fig. 1(f)).

3. Numerical results

3.1. Simulated fMRI dataset

The SimTB toolbox¹ Erhardt et al. (2012) is applied to synthesize multi-subject fMRI datasets in order to evaluate the JpJI-sICA algorithm (the results for JpJI-tICA are similar to JpJI-sICA). In Fig. 2(a) and (b), an example of multi-subject fMRI datasets with JpJI-MDM source model in spatial and temporal approaches are shown. In spatial approach, sources are uncorrelated activated brain regions with $C_1 = 2$, $C_2 = 2$, $C_3 = 1$, $W = 64 \times 64$ and $K = \text{number of subjects} = 10$ (Fig. 2(a)). In temporal approach, sources are uncorrelated time-courses with $C_1 = 1$, $C_2 = 2$, $C_3 = 0$, $W = 150$, and $K = \text{number of seeds} = 16$ (Fig. 2(b)). In both approaches, there are two clusters of subjects with the same partially-joint sources.

In this study, we set $[\alpha_2, \alpha_3, \alpha_4] = [0.5, 0.75, 1]$. Note that in Pakravan and Shamsollahi (2018), different weights settings have been tested, and it has been shown that different values for α can slightly affect the performance of the extraction algorithm. Here, we set these weights based on the results of Pakravan and Shamsollahi (2018). In order to estimate C , we employ Bayesian information criterion (Schwarz et al., 1978).

We have designed two experiments to evaluate the performance of JpJI-sICA algorithm. In the first and second experiment, we assume that

¹ This toolbox is available at <http://mialab.mrn.org/software/simtb/> (accessed: 20.02.18).

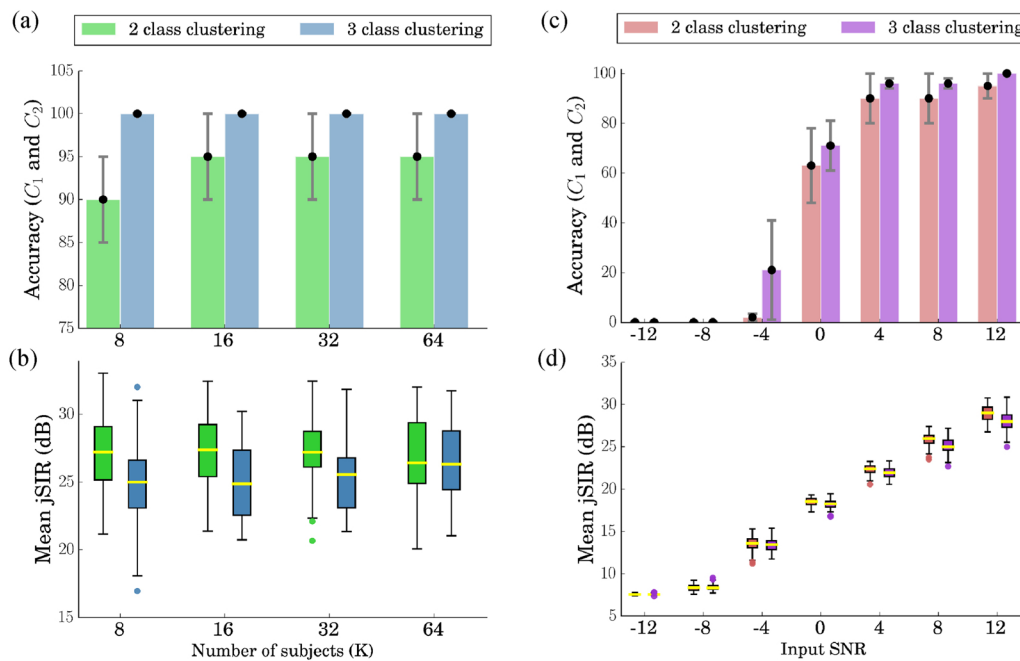


Fig. 4. Performance of the JpJI-sICA algorithm for 2-class and 3-class clustering versus (a,b) the number of subjects and (c,d) SNR of observations in dB in terms of (a,c) its mean jSIR in dB and (b,d) accuracy to estimate the number of sources (joint and partially-joint).

there are only two (referred to as 2-class clustering) and three (referred to as 3-class clustering) sets of subjects which have similar partially-joint sources, respectively. We have used two evaluation metrics, (1) computing correlation between the real and estimated sources (jSIR) in dB and (2) determining the correct type of each source, accuracy (C_1 and C_2), in percent.

The accuracy of estimating the number of joint and partially-joint sources are shown in Fig. 3 versus $\sigma_{similarity}$ ($K = 10$, $C_1 = C_2 = 1$, $C_3^{(k)} = 1$, $k = 1, \dots, K$). As it can be seen for very low values of $\sigma_{similarity}$ ($\sigma_{similarity} \leq 0.1$), the algorithm determines sources randomly as joint or partially-joint. On the other hand, the algorithm determines that all sources are individual for very high values of $\sigma_{similarity}$ ($10^4 \leq \sigma_{similarity}$). Therefore the accuracy of estimating C_1 and C_2 is zero ($Acc(C_1, C_2) = 0$). For $0.5 < \sigma_{similarity} < 100$, the rules in determining the type of sources always work correctly and we have $Acc(C_1, C_2) = 100$.

Fig. 4(a) and (b) represent jSIR and accuracy (C_1 and C_2) for 2-class and 3-class clustering experiments versus different number of subjects. The results are obtained from 100 Monte Carlo runs in which C_1 and C_2 are selected randomly to simulate source data ($C_3 = 0$). As it can be seen the algorithm can extract spatial sources with mean jSIR of 27 dB and 25 dB, and its accuracy to determine the type of each source is 95% and 100% for 2-class and 3-class clustering scenarios, respectively.

We also investigate the performance of JpJI-sICA for noisy observations. Note that a white Gaussian noise is added to the observations for noisy observations. Fig. 4(c) and (d) represent jSIR and accuracy (C_1 and C_2) for 2-class and 3-class clustering experiments versus different input signal to noise ratios (SNR) in dB. As it can be seen the increase of SNR improves the accuracy (C_1 and C_2) (Fig. 4(c)) and mean jSIR (Fig. 4(d)).

3.2. Real fMRI dataset

In this section, we analyze the social brain dataset (Richardson et al., 2018), which investigates the development of brain regions that are involved in thinking about the bodies of others such as pain (Pain matrix) and minds of others such as beliefs and emotions (theory of mind). Two main findings are reported in Richardson et al. (2018): (i)

Theory of Mind and pain matrix are functionally distinct by age 3 years old, and (ii) functional specialization in these networks increases throughout childhood. Note that this data was obtained from the Openneuro data repository (Gorgolewski et al., 2017). Its accession number is ds000228.²

fMRI stimuli: A large sample of children ($n = 122$, 3–12 years) and adults ($n = 33$) watched a 5.6-min animated movie (Reher, 2009) (a silent version of “Partly Cloudy” movie) during fMRI scanning.

fMRI data acquisition: Structural and functional MRI data of whole-brain have been recorded on a 3-Tesla scanner (Siemens Tim Trio) at the Athinoula A. Martinos Imaging Center at MIT. For functional scans, images were collected with Echo-Planar Imaging factor of 64, Repetition Time of 2000 ms, Echo Time of 30 ms, and flip angle of 90°. Furthermore, T1-weighted structural images have been recorded in 176 interleaved sagittal slices with isotropic voxels of 1 mm, where Field-of-View of the adult coil and kid coils were 256 mm² and 192 mm², respectively.

fMRI data analysis: fMRI data have been preprocessed based on the following steps: registering functional images to the first image of the run; registering that image to each participant’s anatomical image, normalizing each participant’s anatomical image to the Montreal Neurological Institute template, smoothing all data using a Gaussian filter (5 mm kernel) Richardson et al. (2018), and denoising BOLD signals with identifying artifact time points using the ART toolbox (Whitfield-Gabrieli et al., 2011). Note that the first five image volumes were removed to avoid T1 equilibration effects.

In Richardson et al. (2018), the authors have used the regain of interests (ROIs) of theory of mind and pain matrix group which have been obtained in Julian et al. (2012). The brain regions of theory of mind include dorso-, middle-, and ventromedial prefrontal cortex, bilateral temporoparietal junction, and precuneus. Furthermore, the brain regions of the pain matrix include dorsal anterior middle cingulate cortex, insula, and secondary sensory cortex, and bilateral medial frontal gyrus. Time-courses from all voxels within an ROI were

²This dataset is available at: <https://openneuro.org/datasets/ds000228/versions/00001> (accessed: 02.08.18) with <https://doi.org/10.5072/FK2V69GD88>.

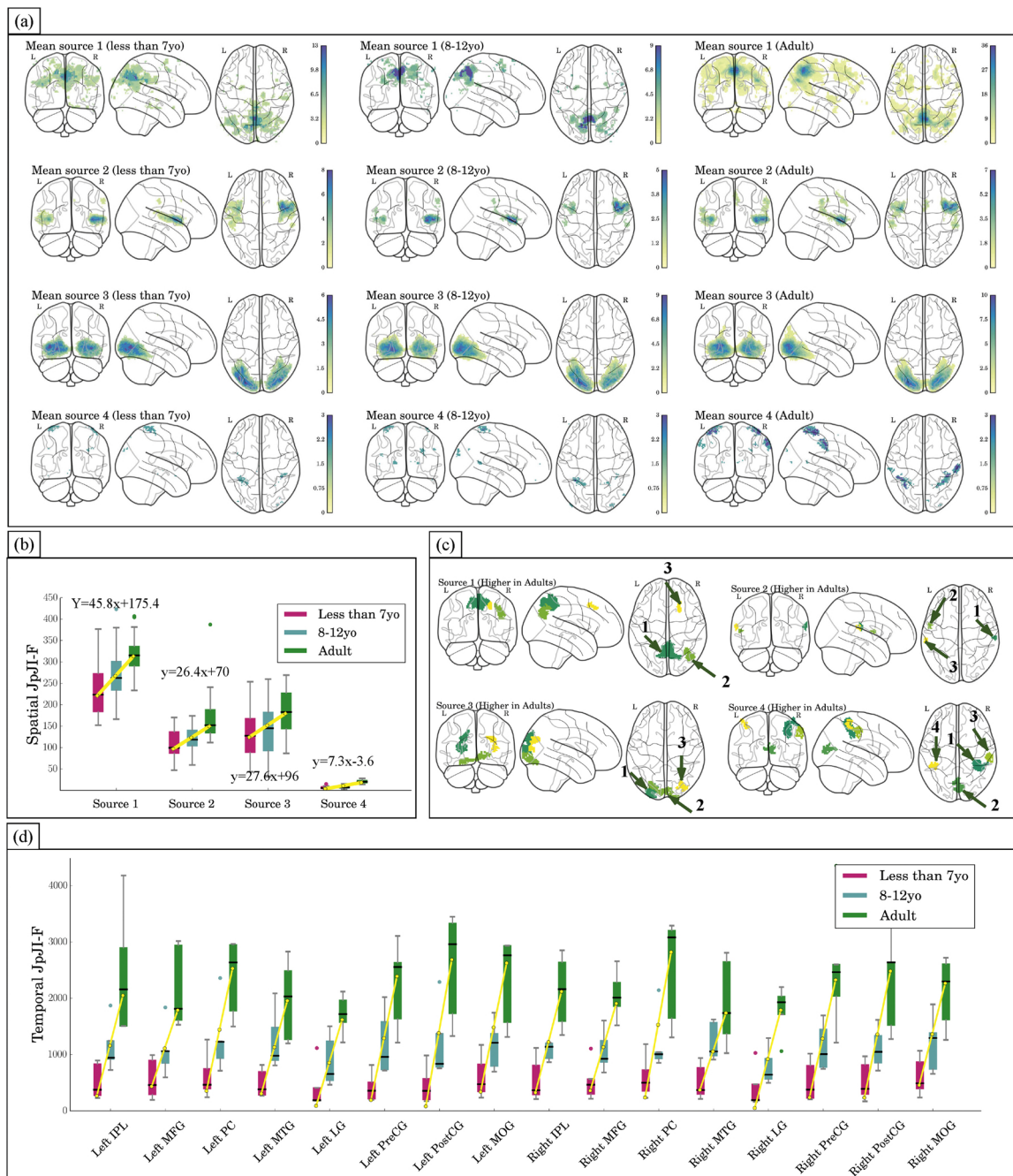


Fig. 5. (a) Spatial distribution of significant joint sources ($p < 0.05$ FDR corrected) of 155 subjects extracted by using the JpJI-sICA algorithm, (b) spatial JpJI-F for each extracted spatial source and different groups of subjects, and (c) map of significant clusters in source 1,2,3 and 4 (d) temporal JpJI-F of extracted temporal sources for each ROI and each group of subjects.

averaged to have one time-course per group ROI. The within-network theory of mind (pain matrix) correlations were the average correlation of each theory of mind (pain matrix) ROI with all other ToM (Pain) ROIs, and the across-network correlations were the average correlation of each theory of mind ROI with each pain matrix ROI.

Results: In Richardson et al. (2018), the authors showed that adults in comparison of children have greater within-network correlations between ToM and pain networks. Furthermore, they concluded that after the age of 3 years the ToM and pain matrix brain regions can be considered as specialized and distinct networks because of low across-network correlations. The authors have further investigated the BOLD time-courses and movie frames to indicate which brain regions are related to the pain matrix or ToM network.

In this study, we have performed additional fMRI preprocessing steps for each subject by using the AFNI (Analysis of Functional Neuro-Images) toolbox (Cox, 1996). The following fMRI preprocessing steps are applied: (i) slice-timing is corrected by applying heptic interpolation (3dTshift function), (ii) BOLD signals are filtered and spikes are removed (3dBandpass function with fbot = 0.009), and (iii) fMRI images are smoothed by using a Gaussian filter with 6 mm kernel (3dmerge function).

We have applied the JpJI-sICA algorithm on the preprocessed fMRI data of 155 subjects to extract 5 independent components ($K = 155$ and $C = 5$). In this approach, we set the number of time points in BOLD signals to the number of observation mixtures ($N = 168$) and the number of voxels as the length of latent source ($W = 79 \times 95 \times 68$). It

Table 1
The number, size, center of mass and name of significant clusters in extracted partially-joint sources for “social brain” dataset.

	Number	Size	Cluster CM [x,y,z]	Cluster name	Cluster function
Source 1 (Higher in Adults)	1	1333	-2.9 + 59.6 + 51.6	Right Precuneus (PC)	Theory of mind network (Gallagher and Frith, 2003; Dougherty et al., 2003)
	2	368	-41.3 + 68.2 + 34.9	Right Middle Temporal Gyrus (MTG)	Theory of mind network (Schurz et al., 2014)
	3	110	-23.1 - 20.9 + 46.0	Right Middle Frontal Gyrus (MFG)	Pain Matrix (Gallagher and Frith, 2003; Zaki et al., 2016)
Source 2 (Higher in Adults)	1	47	-65.1 + 23.0 + 20.5	Right Inferior Parietal Lobule (IPL)	Theory of mind network (Gallagher and Frith, 2003; Dapretto et al., 2006; Saxe and Kanwisher, 2003)
	2	38	+55.6 + 0.2 + 11.4	Left Precentral Gyrus (PreCG)	-
	3	35	+63.0 + 27.0 + 18.6	Left Inferior Parietal Lobule (IPL)	Theory of mind network (Gallagher and Frith, 2003; Dapretto et al., 2006; Saxe and Kanwisher, 2003)
Source 3 (Higher in Adults)	1	523	+24.2 + 93.6 + 20.9	Left Middle Occipital Gyrus (MOG)	A visual association area (Kaas, 1996)
	2	458	+4.7 + 90.0 - 9.6	Left Lingual Gyrus (LG)	Encoding of complex images (Machielens et al., 2000)
	3	266	-33.0 + 83.6 + 20.7	Right Middle Occipital Gyrus (MOG)	A visual association area (Kaas, 1996)
Source 4 (Higher in Adults)	1	467	-39.8 + 39.8 + 52.6	Right Inferior Parietal Lobule (IPL)	Theory of mind network (Gallagher and Frith, 2003; Dapretto et al., 2006; Saxe and Kanwisher, 2003)
	2	253	-3.4 + 78.5 + 12.3	Right Lingual Gyrus (LG)	Encoding of complex images (Machielens et al., 2000)
	3	162	-60.0 + 24.6 + 45.4	Right Postcentral Gyrus (PostCG)	-
	4	119	+43.1 + 40.3 + 59.4	Left Inferior Parietal Lobule (IPL)	Theory of mind network (Gallagher and Frith, 2003; Dapretto et al., 2006; Saxe and Kanwisher, 2003)

is worth mentioning that we have checked different numbers for components, but for numbers bigger than 5, the sources had no extra and useful information. Furthermore, the fifth extracted sources of all subjects are individual sources with low JpJI-F (less than 1). Fig. 5(a) show the mean spatial distribution of the first four significant extracted spatial independent components (FDR corrected p -value of $p < 0.05$).

We have arranged subjects in three groups based on their age: less than 7 years old ($N_{sub} = 88$), 8 to 12 years old ($N_{sub} = 34$), and adults ($N_{sub} = 33$). As mentioned, one of the main advantages of the algorithm is automatic grouping of the extracted sources across subjects by utilizing a measure during the optimization process. This measure for each c and k is based on the shape of extracted sources (represented by cumulants) and $n_{Kc,k}$. Fig. 5(b) shows the mean spatial JpJI-F of each group of subjects for each extracted source. As shown, we have regressed a line on the mean spatial JpJI-F of all sources. For sources 1, 2, 3 and 4, the slope of the best fitted line is 45.8 ($y = 45.8x + 175.4$), 26.4 ($y = 26.4x + 70$), 27.6 ($y = 27.6x + 96$), and 7.3 ($y = 7.3x + 3.6$), respectively. Here x is the index of subject groups and y is the JpJI-F. This means that the spatial JpJI-F of subjects increases throughout childhood.

Fig. 5(c) represents the map of significant clusters in the extracted spatial sources with this null hypothesis that for each voxel, the mean of source values in adults is equal to or less than the mean of source values in subjects with age less than 12 ($p < 0.05$ FDR corrected). As can be seen, in each extracted sources, some clusters are significantly higher in adults. Therefore, we can conclude that all four extracted sources are partially-joint sources; $C_1 = 0$, $C_2 = 4$ and $C_3 = 1$. It should be noted that in all 4 extracted sources and all subjects, the spatial JpJI-F is bigger than 1. The significant clusters extracted in each map are numbered in Fig. 5(c), and the number, size, center of mass (CM) as its seed in RAI order, name in TLRC space, and function are listed in Table 1. These results are obtained by using “whereami” and “clusterize” functions in the AFNI software.

The results show that Precuneus, right Middle Temporal Gyrus, right Middle Frontal Gyrus, left/right Inferior Parietal Lobule, left Precentral Gyrus, left/right Middle Occipital Gyrus, left/right Lingual Gyrus and right Postcentral Gyrus have higher activity in Adults. The extracted brain regions are consistent with Julian et al. (2012), Saxe and Kanwisher (2003), where in the original study (Richardson et al., 2018), predefined ROIs from Julian et al. (2012) have been used. However, the algorithm can extract activated and uncorrelated ROIs which their spatial JpJI-F increases with the age of subjects.

We have also applied three separate JpJI-tICA algorithms for each group of subjects. We assume 16 seeds (Fig. 5(d)) as datasets ($K = 16$), and set $C = 5$. It is worth mentioning that we have checked different numbers for temporal components (C), and the results for low values were similar because we wanted to extract only powerful joint temporal sources to measure the global jointness between ROIs. To compute the time-course of each seed, we have applied the “3dmaskave” function in AFNI toolbox. We have concatenated the seed’s time-course of all subjects in a matrix as the observation matrix ($W = 168$).

In Fig. 5(d), the temporal JpJI-F for each ROI and each group of subjects are presented. Note that all of the slopes of fitted lines are between 650 and 1300. Temporal JpJI-F represents the amounts of extracted temporal sources in each group of subjects and Fig. 5(d) shows that this feature is greater in adults, which is consistent with Richardson et al. (2018). It is worth mentioning that since the timing information of stimuli was not available (due to the complexity of stimuli), we could not analyze the extracted joint temporal sources to find their relation with stimuli.

The results extracted from both JpJI-sICA and JpJI-tICA algorithms show that joint features (spatial JpJI-F and temporal JpJI-F) are greater in adults and this means that synchronicity in spatial and temporal components increases with the age of subjects Richardson et al. (2018).

It should be noted that the results in the real fMRI dataset show that individual sources are probably kind of noise. Thus, the JpJI-sICA

algorithm can identify nuisance effects of datasets as individual sources which can be removed to improve the quality of data.

4. Discussion

In this study, we use JpJI-s/tICA algorithm to analyze multi-subject fMRI data with JpJI-MDM source model using higher-order cumulants. The algorithm differs from existing data fusion methodologies in that it does not assume only joint sources across subjects. Instead, it assumes JpJI-MDM source model including joint, partially-joint, and individual sources. Furthermore, we introduced spatial and temporal JpJI-F which represents (i) the shape of the extracted source in terms of higher-order cumulants; and (ii) the amount of jointness of that source with other sources in other datasets.

The algorithm has been evaluated by analyzing the simulated and real fMRI dataset. In the simulation study, we showed that the spatial approach of the algorithm can extract spatial sources of simulated fMRI data with mean jSIR of 27 dB and 25 dB, and determines the type of each source with accuracy of 95% and 100% for 2-class and 3-class clustering scenarios, respectively. We also showed that the increase of SNR improves the accuracy of estimating the correct number of joint and partially-joint sources and their mean jSIR.

Furthermore, we analyzed the *social brain* fMRI dataset Richardson et al. (2018) to extract its spatial and temporal joint, partially-joint, and individual sources. This dataset investigates the development of brain regions that are involved in reasoning about others' minds and bodies (theory of mind and pain matrix), in a large sample of children between the ages of 3–7 years old (88 subjects), 8–12 years old (34 subjects), and adults (33 subjects). Subjects watched a movie in which the mental states and physical sensations of the characters are evoked during some events. Analysis of Richardson et al. (2018) showed that the theory of mind and pain matrix are functionally distinct by age 3 years old. It is worth mentioning that the important human ability in social cognition is to reason about other people, specifically, in prediction and interpretation of the behavior of people based on an understanding of their minds which is referred to as “theory of mind” (Saxe and Kanwisher, 2003).

In the original study (Richardson et al., 2018), the predefined region of interests (ROIs) have been used to analyze the dataset, whereas the applied unified algorithm in this study simultaneously extracted activated and uncorrelated ROIs which are the spatial joint and partially-joint sources. The extracted ROIs were involved in reasoning about the contents of other people's minds. The algorithm also determined their spatial JpJI-F without additional computations. Using extracted spatial sources, some seeds were selected and their temporal JpJI-F were computed. After extracting the spatial sources as ROIs, we used spatial JpJI-F to determine the type of those ROIs (joint, partially-joint, or individual). If the JpJI-F of a source in different groups of subjects is significantly different, it means that the source is a partially-joint source. In the next step, *two-sided t-test* with FDR corrected *p*-value of $p < 0.05$ was applied on the activated voxels in partially-joint sources to find significant clusters among the groups of subjects. We expected that only in partially-joint sources, significant clusters can be found.

Based on the results obtained from real fMRI data, we observed several partially-joint sources. In the “*social brain dataset*” we had $K = 155$ and $C = 5$ in spatial approach. The output of the algorithm was 5 sources for each subject ($C_1 = 0$, $C_2 = 4$ and $C_3 = 1$) and JpJI-F. We could fit a line with a positive slope on the spatial JpJI-F of grouped subjects concerning their age in each partially-joint source. The fitted line indicates that by increasing the age of subjects, the spatial JpJI-F is approximately increasing. Furthermore, the significant clusters (brain regions) in partially-joint sources were in Precuneus, bilateral Inferior Parietal Lobule, bilateral Lingual Gyrus, bilateral Middle Occipital Gyrus, and Right Middle Frontal/Temporal Gyrus.

In the temporal approach, we had $K = 16$ and $C = 5$ and three separate JpJI-tICA. We investigated the temporal JpJI-F to determine the

global jointness of ROIs in each group of subjects. In our real study, we only wanted to evaluate the visibility of algorithm in extracting joint and partially-joint sources of some available datasets.

Our results on the real dataset were consistent with the existing meta-analysis studies. We showed that spatial and temporal JpJI-F in the theory of mind regions of brain increases with the age of subjects. In future works, our algorithms can be used to investigate real multi-subject fMRI datasets in a meta-analysis with further details.

5. Conclusions

In this paper, we have applied a source model (JpJI-MDM) to analyze multi-subject brain imaging datasets by considering three types of sources (joint, partially-joint, and individual sources). Furthermore, a new algorithm is presented to analyze multi-subject datasets based on the JpJI-MDM source model. In this algorithm, a deflation framework is employed to extract spatial and temporal sources across multiple datasets, and sources of each dataset are extracted one-by-one by maximizing the cost function of the algorithm. Higher-order cumulants are selected as the base of the cost function because the local convergence of higher-order cumulants is not affected by the distributions of sources with non-zero cumulants. The results from both simulated and real fMRI data showed the benefits of the algorithm as either a complementary or alternative method for the inference of fMRI group data. Furthermore, the JpJI-sICA and JpJI-tICA algorithms can provide a useful interpretation of multi-subject fMRI data and help to deal with more complex and realistic source models.

References

- Adali, T., Anderson, M., Fu, G.-S., 2014. Diversity in independent component and vector analyses: identifiability, algorithms, and applications in medical imaging. *IEEE Signal Process. Mag.* 31, 18–33.
- Beckmann, C.F., DeLuca, M., Devlin, J.T., Smith, S.M., 2005. Investigations into resting-state connectivity using independent component analysis. *Philos. Trans. R. Soc. B Biol. Sci.* 360, 1001–1013.
- Calhoun, V.D., Adali, T., 2006. Unmixing fmri with independent component analysis. *IEEE Eng. Med. Biol. Mag.* 25, 79–90.
- Calhoun, V.D., Adali, T., McGinty, V., Pekar, J.J., Watson, T.G., 2001a. Pearson, fmri activation in a visual-perception task: network of areas detected using the general linear model and independent components analysis. *NeuroImage* 14, 1080–1088.
- Calhoun, V.D., Adali, T., Pearson, G.D., Pekar, J.J., 2001b. A method for making group inferences from functional mri data using independent component analysis. *Hum. Brain Mapp.* 14, 140–151.
- Calhoun, V.D., Adali, T., Pearson, G., Pekar, J.J., 2001c. Spatial and temporal independent component analysis of functional mri data containing a pair of task-related waveforms. *Hum. Brain Mapp.* 13, 43–53.
- Calhoun, V.D., Kiehl, K.A., Pearson, G.D., 2008. Modulation of temporally coherent brain networks estimated using ica at rest and during cognitive tasks. *Hum. Brain Mapp.* 29, 828–838.
- Cole, D.M., Smith, S.M., Beckmann, C.F., 2010. Advances and pitfalls in the analysis and interpretation of resting-state fmri data. *Front. Syst. Neurosci.* 4, 8.
- Comon, P., Jutten, C., 2010. *Handbook of Blind Source Separation: Independent Component Analysis and Applications*. Academic Press.
- Cox, R.W., 1996. Afni: software for analysis and visualization of functional magnetic resonance neuroimages. *Comput. Biomed. Res.* 29, 162–173.
- Cruces, S., Cichocki, A., 2003. Combining blind source extraction with joint approximate diagonalization: thin algorithms for ica. *Proceedings of 4th International Symposium on Independent Component Analysis and Blind Signal Separation (ICA2003)* 463–468.
- Dapretto, M., Davies, M.S., Pfeifer, J.H., Scott, A.A., Sigman, M., Bookheimer, S.Y., Iacoboni, M., 2006. Understanding emotions in others: mirror neuron dysfunction in children with autism spectrum disorders. *Nat. Neurosci.* 9, 28.
- Dougherty, D.D., Weiss, A.P., Cosgrove, G.R., Alpert, N.M., Cassem, E.H., Nierenberg, A.A., Price, B.H., Mayberg, H.S., Fischman, A.J., Rauch, S.L., 2003. Cerebral metabolic correlates as potential predictors of response to anterior cingulotomy for treatment of major depression. *J. Neurosurg.* 99, 1010–1017.
- Du, Y., Allen, E.A., He, H., Sui, J., Wu, L., Calhoun, V.D., 2016. Artifact removal in the context of group ica: a comparison of single-subject and group approaches. *Hum. Brain Mapp.* 37, 1005–1025.
- Erhardt, E.B., Allen, E.A., Wei, Y., Eichele, T., Calhoun, V.D., 2012. Simtb, a simulation toolbox for fmri data under a model of spatiotemporal separability. *NeuroImage* 59, 4160–4167.
- Gallagher, H.L., Frith, C.D., 2003. Functional imaging of ‘theory of mind’. *Trends Cognit. Sci.* 7, 77–83.
- Gorgolewski, K., Esteban, O., Schaefer, G., Wandell, B., Poldrack, R., 2017. *Openneuro-4*

- free online platform for sharing and analysis of neuroimaging data. In: Organization for Human Brain Mapping. Vancouver, Canada 1677.
- Hotelling, H., 1936. Relations between two sets of variates. *Biometrika* 28, 321–377.
- Julian, J.B., Fedorenko, E., Webster, J., Kanwisher, N., 2012. An algorithmic method for functionally defining regions of interest in the ventral visual pathway. *Neuroimage* 60, 2357–2364.
- Kaas, J.H., 1996. Theories of visual cortex organization in primates: areas of the third level. *Progress in Brain Research*, vol. 112. Elsevier, pp. 213–221.
- Lock, E.F., Hoadley, K.A., Marron, J.S., Nobel, A.B., 2013. Joint and individual variation explained (jive) for integrated analysis of multiple data types. *Ann. Appl. Stat.* 7, 523.
- Machielsen, W.C., Rombouts, S.A., Barkhof, F., Scheltens, P., Witter, M.P., 2000. Fmri of visual encoding: reproducibility of activation. *Hum. Brain Mapp.* 9, 156–164.
- McKeown, M.J., Makeig, S., Brown, G.G., Jung, T.-P., Kindermann, S.S., Bell, A.J., Sejnowski, T.J., 1998. Analysis of fmri data by blind separation into independent spatial components. *Hum. Brain Mapp.* 6, 160–188.
- Pakravan, M., Bagher Shamsollahi, M., 2019. Joint, Partially-joint, and Individual Independent Component Analysis in Multi-Subject fMRI Data. , arXiv e-prints. arXiv:1909.03676.
- Pakravan, M., Shamsollahi, M.B., 2018. Extraction and automatic grouping of joint and individual sources in multi-subject fmri data using higher order cumulants. *IEEE J. Biomed. Health Inform.*
- Pamilo, S., Malinen, S., Hlushchuk, Y., Seppä, M., Tikka, P., Hari, R., 2012. Functional subdivision of group-ica results of fmri data collected during cinema viewing. *PLoS ONE* 7, e42000.
- S.P.D. Reher, K. (Producer), 2009. Partly cloudy [motion picture], United States: Pixar Animation Studios and Walt Disney Pictures.
- Richardson, H., Lisandrelli, G., Riobueno-Naylor, A., Saxe, R., 2018. Development of the social brain from age three to twelve years. *Nat. Commun.* 9, 1027.
- Saad, Y., 2011. *Numerical Methods for Large Eigenvalue Problems: Revised Edition*, vol. 66 Siam.
- Saxe, R., Kanwisher, N., 2003. People thinking about thinking people: the role of the temporo-parietal junction in “theory of mind”. *Neuroimage* 19, 1835–1842.
- Schurz, M., Radua, J., Aichhorn, M., Richlan, F., Perner, J., 2014. Fractionating theory of mind: a meta-analysis of functional brain imaging studies. *Neurosci. Biobehav. Rev.* 42, 9–34.
- Schwarz, G., et al., 1978. Estimating the dimension of a model. *Ann. Stat.* 6, 461–464.
- Sohn, W.S., Yoo, K., Lee, Y.-B., Seo, S.W., Na, D.L., Jeong, Y., 2015. Influence of roi selection on resting state functional connectivity: an individualized approach for resting state fmri analysis. *Front. Neurosci.* 9, 280.
- Whitfield-Gabrieli, S., Nieto-Castanon, A., Ghosh, S., 2011. *Artifact detection tools (art)*. Camb. Ma. Release Version 7 11.
- Wu, L., Caprihan, A., Bustillo, J., Mayer, A., Calhoun, V., 2018. An approach to directly link ica and seed-based functional connectivity: application to schizophrenia. *NeuroImage* 179, 448–470.
- Zaki, J., Wager, T.D., Singer, T., Keyesers, C., Gazzola, V., 2016. The anatomy of suffering: understanding the relationship between nociceptive and empathic pain. *Trends Cognit. Sci.* 20, 249–259.
- Zhou, G., Cichocki, A., Zhang, Y., Mandic, D.P., 2016. Group component analysis for multiblock data: common and individual feature extraction. *IEEE Trans. Neural Netw. Learn. Syst.* 27, 2426–2439.